

Search for Charged Higgs Bosons through Vector-Like Top Quark Pair Production at the LHC

A. ARHRIB^{1,2*}, R. BENBRIK^{3†}, M. BERROUJ^{3‡}, M. BOUKIDI^{3§}, B. MANAUT^{4¶}

- ¹ *Université Abdelmalek Essaadi, Faculty of sciences and techniques, B. 416, Tangier, Morocco.*
² *Department of Physics and Center for Theory and Computation, National Tsing Hua University, Hsinchu, Taiwan 300.*
³ *Polydisciplinary Faculty, Laboratory of Fundamental and Applied Physics, Cadi Ayyad University, Sidi Bouzid, B.P. 4162, Safi, Morocco.*
⁴ *Polydisciplinary Faculty, Laboratory of Research in Physics and Engineering Sciences, Team of Modern and Applied Physics, Sultan Moulay Slimane University, Beni Mellal, Morocco.*

Abstract

We investigate the production and decay of a vector-like top partner (T) with charge $2/3$ within the Two Higgs Doublet Model Type II (2HDM-II) extended by a vector-like quark (VLQ) doublet (TB). This study focuses on the decay sequence where the T quark produces a charged Higgs boson (H^+) and a bottom quark, followed by the H^+ decay into a top and bottom quark, due to the small branching ratio for $H^+ \rightarrow \tau\nu$ in the studied region. Previous research [Phys.Rev.D109,055016] has shown that the decay pathway $T \rightarrow H^+b$ followed by $H^+ \rightarrow tb$ is dominant across a significant portion of the parameter space. We analyze the collider process $pp \rightarrow T\bar{T} \rightarrow (bH^+)(\bar{b}H^-) \rightarrow (b(tb))(\bar{b}(\bar{t}\bar{b}))$, resulting in final states enriched with bottom quarks. Our findings highlight this channel as a promising avenue for discovering the new top partner and charged Higgs boson, offering substantial detection potential across a broad parameter space.

*aarhrib@gmail.com

†r.benbrik@uca.ac.ma

‡mbark.berrouj@ced.uca.ma

§mohammed.boukidi@ced.uca.ma

¶b.manaut@usms.ma

1 Introduction

The discovery of a charged spin-0 boson, H^\pm , would strongly indicate physics beyond the Standard Model (BSM), as the Standard Model (SM) does not predict such particles. While the SM includes charged spin-1 bosons and a chargeless spin-0 boson, it lacks a charged spin-0 boson. Consequently, the search for charged Higgs bosons has intensified at particle accelerators like the Large Hadron Collider (LHC) at CERN. Despite extensive search efforts, no H^\pm signals have been observed. Results from ATLAS and CMS experiments have excluded large areas of the parameter space for BSM scenarios that include these particles, particularly within the framework of the 2-Higgs Doublet Model Type II (2HDM-II) and its Supersymmetric variant, the Minimal Supersymmetric Standard Model (MSSM).

Vector-like quarks (VLQs) are heavy spin-1/2 particles that form color triplets and have identical Electro-Weak (EW) quantum numbers for their left- and right-handed couplings, unlike SM quarks. VLQs are predicted by several theoretical models, including those with gauged flavor symmetries [1–4], non-minimal Supersymmetric scenarios [5–10], Grand Unified Theories [11, 12], little Higgs models [13, 14], and Composite Higgs models [15–23]. These models often predict VLQs as partners of the third generation of quarks, mixing with top and bottom quarks. If VLQs have masses within the LHC’s kinematic reach, they can be observed in various final states [24–58]. Several of these states have already been investigated by the ATLAS and CMS collaborations [59–84]. Moreover, VLQs have the potential to explain various experimental anomalies, including the W mass discrepancy [85–88].

Previous research [89, 90] has established a comprehensive framework for searching for vector-like top and bottom partners in the alignment limit of the 2HDM-II, exploring all possible representations, including singlets, doublets, and triplets. These studies have focused on the decay modes of VLQs into exotic particles ($Q \rightarrow q\Phi$ ($\Phi = H, A, H^\pm$)). Other work [91] has examined the effects of incorporating VLQs into the 2HDM-II, particularly on the limits from B physics on the charged Higgs boson, and studied the phenomenology of charged Higgs production from vector-like top partner T (VLT).

Building on these findings, this study expands the analysis within the 2HDM-II framework by incorporating a VLQ doublet (TB) and employing Monte Carlo (MC) simulations. We concentrate on the pair production of the VLT and its subsequent decay into a charged Higgs boson (H^+) and a bottom quark. The H^+ further decays into a top and bottom quark. This decay pathway, $T \rightarrow bH^+ \rightarrow b(tb)$, dominates a substantial portion of the parameter space. Our findings demonstrate that this channel is promising for detecting both the top partner and the charged Higgs boson, offering significant detection potential across a wide parameter space.

2 Framework

In this section, we only provide a brief overview of the 2HDM-II+ TB realisation. We begin by recalling the well-known \mathcal{CP} -conserving 2HDM scalar potential for two doublet fields (Φ_1, Φ_2) with a discrete \mathbb{Z}_2 symmetry, $\Phi_1 \rightarrow -\Phi_1$, which is softly violated by dimension-2 terms [92, 93]:

$$\begin{aligned} \mathcal{V} = & m_{11}^2 \Phi_1^\dagger \Phi_1 + m_{22}^2 \Phi_2^\dagger \Phi_2 - \left(m_{12}^2 \Phi_1^\dagger \Phi_2 + \text{h.c.} \right) + \frac{1}{2} \lambda_1 \left(\Phi_1^\dagger \Phi_1 \right)^2 + \frac{1}{2} \lambda_2 \left(\Phi_2^\dagger \Phi_2 \right)^2 \\ & + \lambda_3 \Phi_1^\dagger \Phi_1 \Phi_2^\dagger \Phi_2 + \lambda_4 \Phi_1^\dagger \Phi_2 \Phi_2^\dagger \Phi_1 + \left[+ \frac{1}{2} \lambda_5 \left(\Phi_1^\dagger \Phi_2 \right)^2 + \text{h.c.} \right]. \end{aligned} \quad (1)$$

Here, all parameters are real. The two complex scalar doublets $\Phi_{1,2}$ can be rotated into a basis, $H_{1,2}$, where only one acquires a Vacuum Expectation Value (VEV). Using the minimization conditions

of the potential for EW Symmetry Breaking (EWSB), the 2HDM can be fully described by seven independent parameters: m_h , m_H , m_A , m_{H^\pm} , $\tan\beta(=v_2/v_1)$, $\sin(\beta - \alpha)$, and the soft-breaking parameter m_{12}^2 .

To prevent significant tree-level Flavour Changing Neutral Currents (FCNCs), the 2HDM allows for four distinct Yukawa configurations, determined by the implementation of the \mathbb{Z}_2 symmetry in the fermion sector¹. These configurations are: Type-I, where only Φ_2 couples to all fermions; Type-II, where Φ_2 couples to up-type quarks, while Φ_1 couples to charged leptons and down-type quarks; Type-Y (Flipped), where Φ_2 couples to charged leptons and up-type quarks, and Φ_1 couples to down-type quarks; and Type-X (Lepton Specific), where Φ_2 couples to quarks, and Φ_1 couples to charged leptons.

Next, we discuss the VLQ component of the model, focusing on the gauge-covariant multiplet (TB) . The fields T and B in this multiplet have electric charges of $2/3$ and $-1/3$, respectively. The representation of these fields under the SM gauge group is detailed in Table 1. Specifically, the T field is a triplet under the color group $SU(3)_C$ and a singlet under the electroweak group $SU(2)_L \times U(1)_Y$. Both the right-handed (RH) and left-handed (LH) components, denoted as TL, R^0 , possess identical electroweak and color quantum numbers.

The mixing of VLQs with the first and second generations of SM quarks is heavily constrained by low-energy physics measurements. One prominent example of such constraints arises from Electroweak Precision Observables (EWPOs), including oblique parameter corrections. These corrections, which impact quantities such as the W^\pm boson mass (m_{W^\pm}) and the effective mixing angle ($\sin^2\theta_W$) at higher orders, are sensitive to the presence of VLQs and can impose restrictions on their masses and couplings [86, 94]. Additionally, VLQs, particularly those in the third generation, can influence the properties of top and bottom quarks through fermion mixing [95]. This mixing can have significant implications for processes like the decay of the Z boson into bottom quarks, which has been measured with high precision at the LEP e^+e^- collider at energies near the Z resonance [52, 96]. Deviations from SM predictions in such measurements can provide stringent constraints on the properties of VLQs. Consequently, we focus on scenarios where the VLQs interact exclusively with third-generation SM quarks.

Component fields	(TB)
$U(1)_Y$	$1/6$
$SU(2)_L$	2
$SU(3)_C$	3

TABLE 1: Doublet VLQ representation under the SM gauge group.

In the Higgs basis, the Yukawa Lagrangian can be expressed as follows:

$$-\mathcal{L} \supset y^u \bar{Q}_L^0 \tilde{H}_2 u_R^0 + y^d \bar{Q}_L^0 H_1 d_R^0 + M_u^0 \bar{u}_L^0 u_R^0 + M_d^0 \bar{d}_L^0 d_R^0 + \text{h.c.} \quad (2)$$

where u_R spans (u_R, c_R, t_R, T_R) and d_R spans (d_R, s_R, b_R, B_R) , while $y^{u,d}$ are 3×4 Yukawa matrices. When only the top quark mixes with T , the relationship between mass eigenstates $(T_{L,R})$ and weak eigenstates $(T_{L,R}^0)$ can be described using two 2×2 unitary matrices $U_{L,R}$:

$$\begin{pmatrix} t_{L,R} \\ T_{L,R} \end{pmatrix} = U_{L,R}^u \begin{pmatrix} t_{L,R}^0 \\ T_{L,R}^0 \end{pmatrix} = \begin{pmatrix} \cos\theta_{L,R}^u & -\sin\theta_{L,R}^u e^{i\phi_u} \\ \sin\theta_{L,R}^u e^{-i\phi_u} & \cos\theta_{L,R}^u \end{pmatrix} \begin{pmatrix} t_{L,R}^0 \\ T_{L,R}^0 \end{pmatrix}, \quad (3)$$

¹This study focuses exclusively on the Type-II 2HDM.

where θ is the mixing angle between mass and weak eigenstates, and ϕ is a potential \mathcal{CP} -violating phase, which we will ignore in this work. In the weak eigenstate basis, diagonalizing the mass matrices results in the Lagrangian of the third generation and heavy quark mass terms as follows:

$$\begin{aligned} \mathcal{L}_{\text{mass}} = & - \begin{pmatrix} \bar{t}_L^0 & \bar{T}_L^0 \end{pmatrix} \begin{pmatrix} y_{33}^u \frac{v}{\sqrt{2}} & y_{34}^u \frac{v}{\sqrt{2}} \\ y_{43}^u \frac{v}{\sqrt{2}} & M^0 \end{pmatrix} \begin{pmatrix} t_R^0 \\ T_R^0 \end{pmatrix} \\ & - \begin{pmatrix} \bar{b}_L^0 & \bar{B}_L^0 \end{pmatrix} \begin{pmatrix} y_{33}^d \frac{v}{\sqrt{2}} & y_{34}^d \frac{v}{\sqrt{2}} \\ y_{43}^d \frac{v}{\sqrt{2}} & M^0 \end{pmatrix} \begin{pmatrix} b_R^0 \\ B_R^0 \end{pmatrix} + \text{h.c.}, \end{aligned} \quad (4)$$

where M^0 is a bare mass and the y_{ij} 's are Yukawa couplings. For the doublet case has $y_{34} = 0$. Using standard techniques of diagonalisation, the mixing matrices are obtained by

$$U_L^q \mathcal{M}^q (U_R^q)^\dagger = \mathcal{M}_{\text{diag}}^q, \quad (5)$$

with \mathcal{M}^q the two mass matrices in Eq. (4) and $\mathcal{M}_{\text{diag}}^q$ the diagonalised ones. The mixing angles in the LH and RH sectors are not independent parameters. Using Eq. (5) one can find:

$$\tan \theta_L^q = \frac{m_q}{m_Q} \tan \theta_R^q, \quad (6)$$

with $(q, m_q, m_Q) = (u, m_t, m_T)$ and (d, m_b, m_B) .

Our focus is on the decay of the vector-like top partner (T) into a charged Higgs boson (H^\pm). Below is the expression for the decay width in the 2HDM-II+ TB scenario²:

$$\begin{aligned} \Gamma(T \rightarrow H^\pm b) = & \frac{g^2}{64\pi} \frac{m_T}{M_W^2} \lambda(m_T, m_b, M_{H^\pm})^{1/2} \{ (|Z_{Tb}^L|^2 \cot^2 \beta + |Z_{Tb}^R|^2 \tan^2 \beta) \\ & \times [1 + r_b^2 - r_{H^\pm}^2] + 4r_b \text{Re} Z_{Tb}^L Z_{Tb}^{R*} \}. \end{aligned} \quad (7)$$

Here, $r_x = m_x/m_T$, where x is one of the decay products, and the function $\lambda(x, y, z)$ is defined as:

$$\lambda(x, y, z) \equiv (x^4 + y^4 + z^4 - 2x^2y^2 - 2x^2z^2 - 2y^2z^2), \quad (8)$$

and

$$Z_{Tb}^L = c_L^d s_L^u e^{-i\phi_u} + (s_L^{u2} - s_R^{u2}) \frac{s_L^d}{c_L^u}, \quad Z_{Tb}^R = \frac{m_b}{m_T} \left[c_L^d s_L^u + (s_R^{d2} - s_L^{d2}) \frac{c_L^u}{s_L^d} \right] \quad (9)$$

3 Theoretical and Experimental Bounds

In this section, we outline the constraints used to validate our results.

- **Unitarity** constraints require the S -wave component of the various (pseudo)scalar-(pseudo)scalar, (pseudo)scalar-gauge boson, and gauge-gauge bosons scatterings to be unitary at high energy [97].
- **Perturbativity** constraints impose the following condition on the quartic couplings of the scalar potential: $|\lambda_i| < 8\pi$ ($i = 1, \dots, 5$) [92].

²Detailed analytical calculations of the couplings are provided in the Appendix of Ref. [91].

- **Vacuum stability** constraints require the potential to be bounded from below and positive in any arbitrary direction in the field space, as a consequence, the λ_i parameters should satisfy the conditions as [98, 99]:

$$\begin{aligned}\lambda_1 &> 0, \quad \lambda_2 > 0, \quad \lambda_3 > -\sqrt{\lambda_1 \lambda_2}, \\ \lambda_3 + \lambda_4 - |\lambda_5| &> -\sqrt{\lambda_1 \lambda_2}.\end{aligned}\tag{10}$$

- **Constraints from EWPOs**, implemented through the oblique parameters³, S and T [100], require that, for a parameter point of our model to be allowed, the corresponding $\chi^2(S^{\text{2HDM-II}} + S^{\text{VLQ}}, T^{\text{2HDM-II}} + T^{\text{VLQ}})$ is within 95% Confidence Level (CL) in matching the global fit results [101]:

$$S = 0.05 \pm 0.08, \quad T = 0.09 \pm 0.07, \quad \rho_{S,T} = 0.92 \pm 0.11.$$

Note that unitarity, perturbativity, vacuum stability, as well as S and T constraints, are enforced through the public code 2HDMC-1.8.0⁴ [102].

- **Constraints from the SM-like Higgs-boson properties** are taken into account by using HiggsSignal-3 [103, 104] via HiggsTools [105]. We require that the relevant quantities (signal strengths, etc.) satisfy $\Delta\chi^2 = \chi^2 - \chi^2_{\min}$ for these measurements at 95% CL ($\Delta\chi^2 \leq 6.18$).
- **Constraints from direct searches at colliders**, i.e., LEP, Tevatron, and LHC, are taken at the 95% CL and are tested using HiggsBounds-6 [106–109] via HiggsTools. Including the most recent searches for neutral and charged scalars.
- **Constraints from $b \rightarrow s\gamma$** : To comply with the $b \rightarrow s\gamma$ limit, the mass of the charged Higgs boson is set to exceed 600 GeV. This is based on analyses indicating that incorporating VLQs into the Type-II 2HDM can relax this limit with larger mixing angles. However, constraints from EWPOs limit these angles to smaller values, keeping the charged Higgs mass near 580 GeV, typical for the 2HDM Type-II [91].

4 Numerical Analysis

Parameters	Scanned ranges
m_h	125.09
m_A	[400, 800]
m_H	[400, 800]
m_{H^\pm}	[600, 800]
$s_{\beta-\alpha}$	1
t_β	[1, 20]
m_{12}^2	$m_A^2 \tan \beta / (1 + \tan \beta^2)$
$s_R^{u,d}$	[-0.3, 0.3]
m_T	[1000, 2000]

TABLE 2: 2HDM & VLQs parameters with their scanned ranges. Masses are in GeV.

³A comprehensive discussion on EWPO contributions in VLQs can be found in [90]

⁴The code has been adjusted to include new VLQ couplings, along with the integration of analytical expressions for S_{VLQs} and T_{VLQs} outlined in Ref. [90].

To explore the parameter space for the 2HDM-II+ TB scenario, we conducted a comprehensive numerical scan within the ranges listed in Table 2. Our goal was to identify scenarios⁵ that result in substantial cross-sections for the $4t2b$ final state. All selected points were validated against the theoretical and experimental constraints discussed in previous section.

We used MadGraph5_aMC@NLO [110] to compute the cross-section for the process $pp \rightarrow T\bar{T} \rightarrow 2H^\pm + 2b \rightarrow 4b + 2t$ at $\sqrt{s} = 14$ TeV, utilizing the CTEQ6L1 [111] parton distribution function.

Before presenting the cross-section results, we first show in Fig. 1 the Branching Ratios (\mathcal{BR} s) of $T \rightarrow H^+b$ (left panel) and $H^+ \rightarrow tb$ (right panel) as functions of the VLT mass m_T and m_{H^\pm} , respectively. These plots clearly demonstrate that the production of charged Higgs bosons from the new top partner T can dominate across the mass range $m_T \in [1000, 2000]$ GeV, reaching a maximum \mathcal{BR} of 98%. Similarly, the decay of H^+ into tb is nearly 100% over the selected mass range.

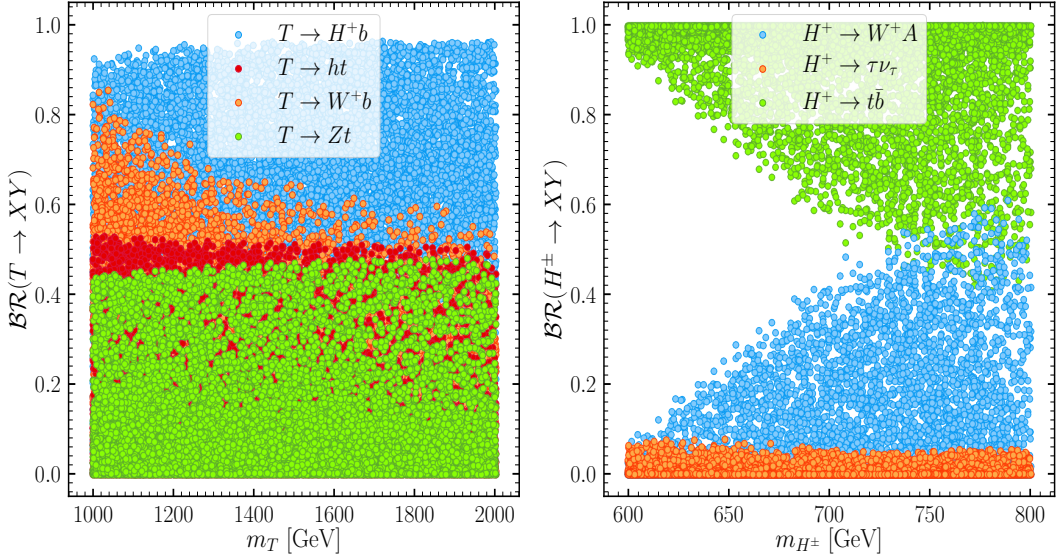


FIGURE 1: Left: $\mathcal{BR}(T \rightarrow XY)$ as a function of m_T , with $XY = H^+b$ light blue, ht red, W^+b orange and Zt green. Right: $\mathcal{BR}(H^\pm \rightarrow XY)$ as a function of m_{H^\pm} , with $XY = W^+A$ light blue, $\tau\nu$ orange, and $t\bar{b}$ orange.

Fig. 2 illustrates the distribution of points in the $(m_T, \tan\beta)$ plane, mapped against $\sigma_{T\bar{T}} \times \mathcal{BR}^2(T \rightarrow H^+b) \times \mathcal{BR}^2(H^+ \rightarrow tb)$. The plots indicate that the $4b2t$ signal can reach values up to 100 fb for medium $\tan\beta$ values and $m_T \leq 1000$ GeV. The enhanced TH^+b coupling in this scenario contributes to a significantly larger cross-section for this signature.

From the scanned parameter space, we selected four benchmark points (BPs), highlighted in orange circles in Fig. 2, which exhibit large $4b2t$ cross-sections for varying values of T mass. The details of these BPs are provided in Table 3.

⁵This work specifically focuses on the TB doublet scenario, which is conducive to significant production of charged Higgs bosons (H^\pm) from VLQs. For more details, see [89, 90].

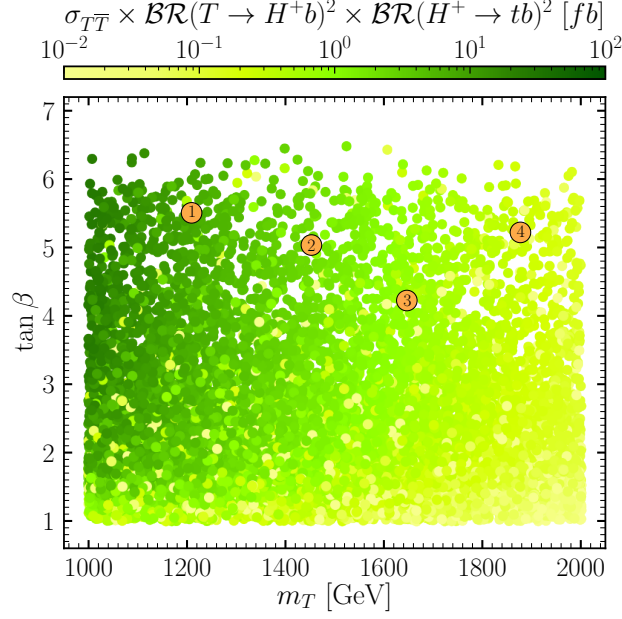


FIGURE 2: $\sigma_{T\bar{T}} \times \mathcal{BR}(T \rightarrow H^+ b)^2 \times \mathcal{BR}(H^+ \rightarrow t\bar{b})^2$ as a function of m_T and $\tan\beta$ for 2HDM-II+ TB . The orange circles indicate our selected BPs.

Parameters	BP ₁	BP ₂	BP ₃	BP ₄
(Masses are in GeV)				
m_h	125.09	125.09	125.09	125.09
m_H	640.62	640.99	655.93	651.30
m_A	639.27	640.51	655.27	648.64
m_{H^\pm}	642.49	648.62	647.40	671.88
t_β	5.51	5.04	4.22	5.22
$s_{\beta-\alpha}$	1	1	1	1
m_T	1209.30	1452.71	1646.60	1877.38
m_B	1217.69	1468.14	1662.59	1888.71
s_L^u	0.00008	0.00659	-0.00706	-0.00221
s_L^d	0.00046	-0.00051	-0.00045	-0.00028
s_R^u	0.00056	0.05536	-0.06717	-0.02405
s_R^d	0.11718	-0.15450	-0.15338	-0.11194
\mathcal{BR} in %				
$\mathcal{BR}(T \rightarrow H^+ b)$	93.98	93.49	91.43	95.19
$\mathcal{BR}(H^+ \rightarrow t\bar{b})$	95.63	96.86	98.33	96.42

TABLE 3: The description of our BPs.

4.1 Signal-Background Analysis

In this section, we present a comprehensive signal-background analysis for the final state involving $4b2t$ at the LHC, using detector simulation. The primary signal process considered is $pp \rightarrow T\bar{T} \rightarrow 2H^\pm + 2b$, followed by $H^\pm \rightarrow t\bar{b}$, with each top quark (t) subsequently decaying into a b -quark, resulting in a final state rich in b -quarks.. Fig. 3 illustrates the Feynman diagrams for

pair production of T (a) and B (b) quarks, and their subsequent decay. Note that both diagrams will yield the same final state ($6b$) after considering the decay of t to bW^+ . However, our analysis focuses only on the diagram involving the vector-like top quark T (a), as the production of charged Higgs bosons from T can reach 98% of \mathcal{BR} , resulting in a significantly larger cross-section compared to B , where the production can achieve a maximum value of 34% [89].

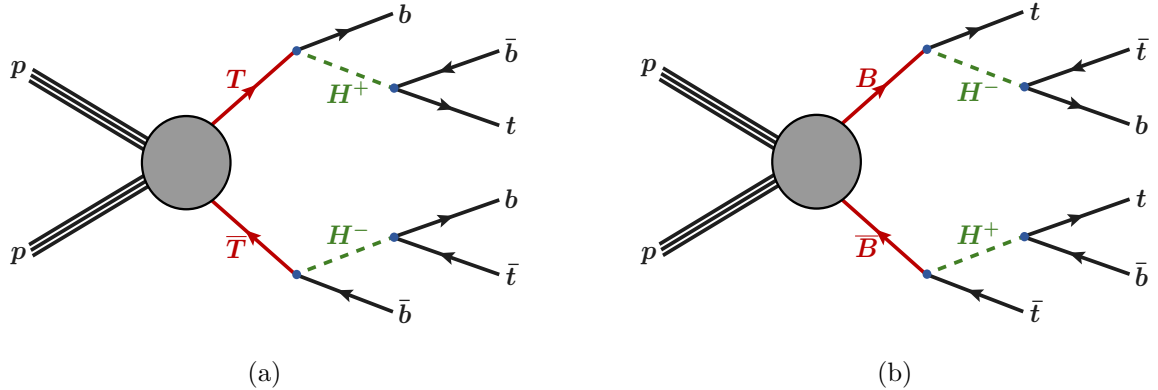


FIGURE 3: Feynman diagrams for pair production of T (a) and B (b) quarks and their subsequent decay into $4b2t$ and $4t2b$ respectively.

Our analysis considers two scenarios: tagging four b -jets ($4b$ analysis) and tagging five b -jets ($5b$ analysis). Cross-sections are determined for events that meet these criteria.

We used `FeynRulesv2.3` [112] to construct the `2HDM-II+TB` model and obtain the `Universal FeynRules Output` [113] model files. Event generation for both signal and background processes was performed using `MadGraph5_aMC@NLO` with `CTEQ6L1` parton distribution functions as discussed earlier. Parton showering and hadronization were carried out using `PYTHIA-8.2` [114], and detector simulation was managed by `Delphes-3.4.2` [115]. Jet reconstruction employed the anti- k_t algorithm [116] with a radius parameter of $R = 0.4$ and $p_T(j) > 20$ GeV. Default b -jet (mis-)tagging efficiencies from the `Delphes` CMS card, based on Ref. [117], were applied.

For higher-order effects, we multiplied the leading-order cross-sections by the highest-order K -factors available in the literature see Table 4. For the signal, we estimated the NNLO K -factor to be 1.42 in the relevant mass range using the `Top++` package [118].

Processes	$b\bar{b}jets$	$b\bar{b}b\bar{b}j$	$t\bar{t}b\bar{b}$	$t\bar{t}t\bar{t}$	$b\bar{b}b\bar{b}b\bar{b}$
K -factor	1.33 [110]	1.4 [119]	1.77 [120]	1.27 [121]	2 [122]

TABLE 4: The K -factors of the QCD corrections for the background processes.

After generating signal and background events, the following selection cuts are applied at the parton level:

1. Events must contain at least four b -jets.
2. b -jets and jets must satisfy the following criteria:
 - $p_T^b > 100$ GeV,
 - $p_T^j > 20$ GeV,

- $|\eta^{b,j}| < 2.5$,
- $\Delta R(x, y) > 0.4$ for the separation between two particles x and y , where $x, y = j, b$.

The numerical values of the input SM parameters are as follows:

$$m_t = 172.6 \text{ GeV}, \quad m_Z = 91.153 \text{ GeV}, \quad \sin^2(\theta_W) = 0.2226, \quad \alpha(m_Z) = 1/127.934 \quad (11)$$

• 4b Analysis

In this analysis, we focus on primary backgrounds involving four high- p_T b -tagged jets, covering $2bjj(j)$, $4b(j)$, $2t2b(j)$, and $4t(j)$ processes. The distributions in Fig. 4 demonstrate the capacity of the analysis variables to differentiate between the signal and the background. The next step involves identifying specific regions within the phase space where the signal displays a significant enhancement relative to the background. By closely examining the kinetic distribution of both the signal and the background, we gain insights into the distinct characteristics of events that occurred during the collision. Among the kinematic variables employed in our analysis, the transverse momentum of b -tagging jets $p_T[b]$, and the total transverse energy of reconstructed b -tagged jets (referred to as sp_T). The cuts applied in our analysis are summarized in Table 5.

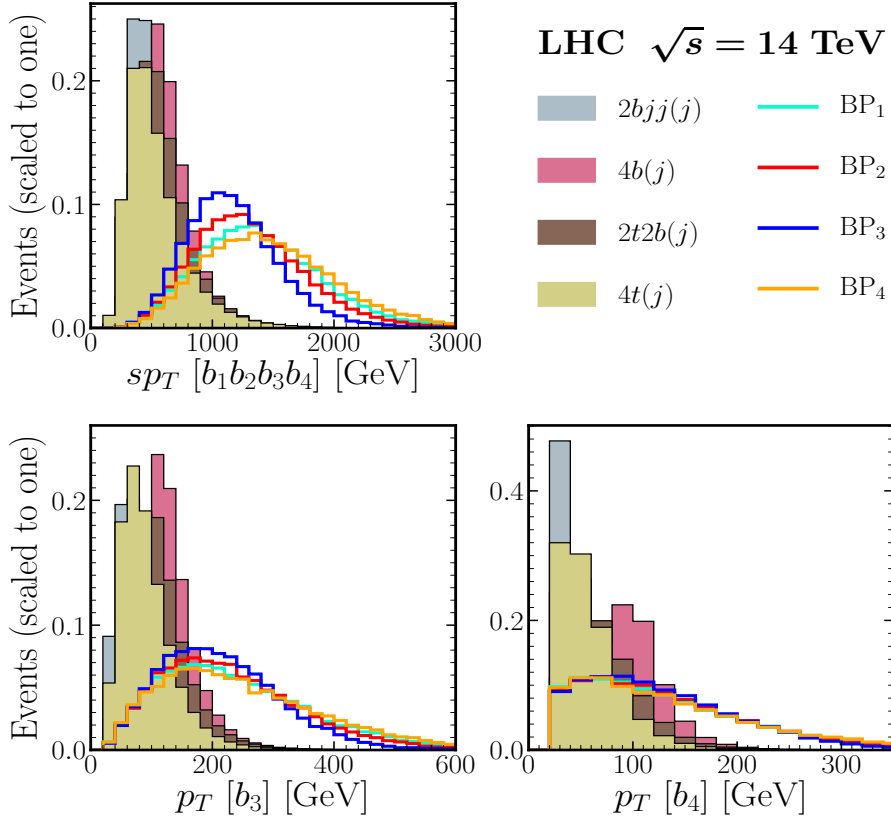


FIGURE 4: $p_T(b_3)$, $p_T(b_4)$, and $sp_T(b_1b_2b_3b_4)$ distributions of the signal BPs (BP₁, BP₂, BP₃, BP₄) and backgrounds at $\sqrt{s} = 14$ TeV.

Cuts	Definition
Cut 1	$\Delta R(b, b) > 0.4$, $\eta(b) < 2.5$
Cut 2	$s_{PT} > 1400$ GeV
Cut 3	$p_T^{b_4} > 140$ GeV $p_T^{b_3} > 250$ GeV

TABLE 5: Set of cuts for the analysis of signal and background events at $\sqrt{s} = 14$ TeV.

Table 6 presents the cut flows applied to both signal BPs and background events at a center-of-mass energy of $\sqrt{s} = 14$ TeV. The results illustrate the effectiveness of the chosen cuts in reducing background influences and enhancing signal isolation. After applying these criteria, the total cut efficiency for the signal becomes notably prominent, achieving values of 7.61%, 10.6%, 11.4%, and 12%. In contrast, the cumulative cut efficiencies for background events are significantly reduced to the order of $\mathcal{O}(10^{-4})$.

Cuts	Signals				Backgrounds			
	BP1	BP2	BP3	BP4	$2bjets$	$4bj$	$2t2bj$	$4tj$
Basic	9.92	1.92	0.74	0.27	309679.46	613.60	288.02	15.65
Cut1	5.52	0.99	0.37	0.12	3471.0	152.8	65.1	3.38
Cut 2	1.30	0.38	0.17	0.065	14.37	1.09	0.795	0.0447
Cut 3	0.76	0.204	0.085	0.032	2.18	0.45	0.20	0.006
Efficiency	7.61%	10.6%	11.4%	12%	$7.05E^{-6}$	$7.49E^{-4}$	$7.05E^{-4}$	$4.39E^{-4}$

TABLE 6: Cut flow of the cross sections (in fb) for the signals and SM backgrounds at the LHC with $\sqrt{s}=14$ TeV with our three typical BPs .

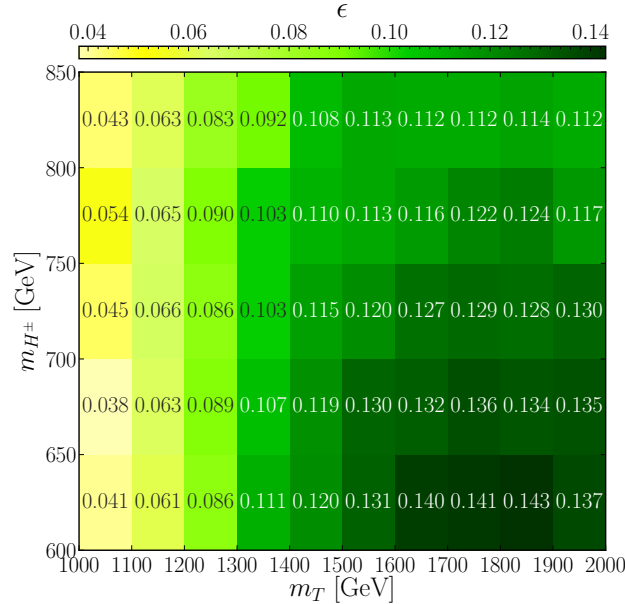


FIGURE 5: Selection efficiency (ϵ) for the signal process in the $4b$ Analysis with 5×10^5 events, utilizing the cut referenced in Table 5 with fixed parameters: $m_H = m_A = 600$ GeV, $\tan \beta = 6$, $s_R^u = 0.05$, and $s_R^d = 0.1$.

In Fig. 5, we depict the selection efficiencies for the signal in the $4b$ analysis. The efficiencies are illustrated in the (m_T, m_{H^\pm}) plane, using fixed parameters: $m_H = m_A = 600$ GeV, $\tan \beta = 6$, $s_R^u = 0.05$, and $s_R^d = 0.1$. The data show an increase in efficiency with rising m_T . Peak efficiency values are concentrated within the m_{H^\pm} mass range of $[600, 650]$ GeV, with the highest efficiencies observed for m_T between $[1600, 1900]$ GeV.

To evaluate the observability of our signal, we use the median significance approach as described in Ref. [123]. We calculate the discovery significance, $\mathcal{Z}_{\text{disc}}$, and the exclusion significance, $\mathcal{Z}_{\text{excl}}$, with the following formulas:

$$\mathcal{Z}_{\text{disc}} = \sqrt{2 \left[(s+b) \ln \left(\frac{(s+b)(1+\delta^2 b)}{b+\delta^2 b(s+b)} \right) - \frac{1}{\delta^2} \ln \left(1 + \delta^2 \frac{s}{1+\delta^2 b} \right) \right]}. \quad (12)$$

$$\mathcal{Z}_{\text{excl}} = \sqrt{2 \left[s - b \ln \left(\frac{s+b+x}{2b} \right) - \frac{1}{\delta^2} \ln \left(\frac{b-s+x}{2b} \right) \right] - (b+s-x) \left(1 + \frac{1}{\delta^2 b} \right)}.$$

where

$$x = \sqrt{(s+b)^2 - 4\delta^2 s b^2 / (1 + \delta^2 b)}.$$

In the limit of $\delta \rightarrow 0$, these expressions simplify to:

$$\begin{aligned} \mathcal{Z}_{\text{disc}} &= \sqrt{2 [(s+b) \ln(1+s/b) - s]}, \\ \mathcal{Z}_{\text{excl}} &= \sqrt{2 [s - b \ln(1+s/b)]}. \end{aligned} \quad (13)$$

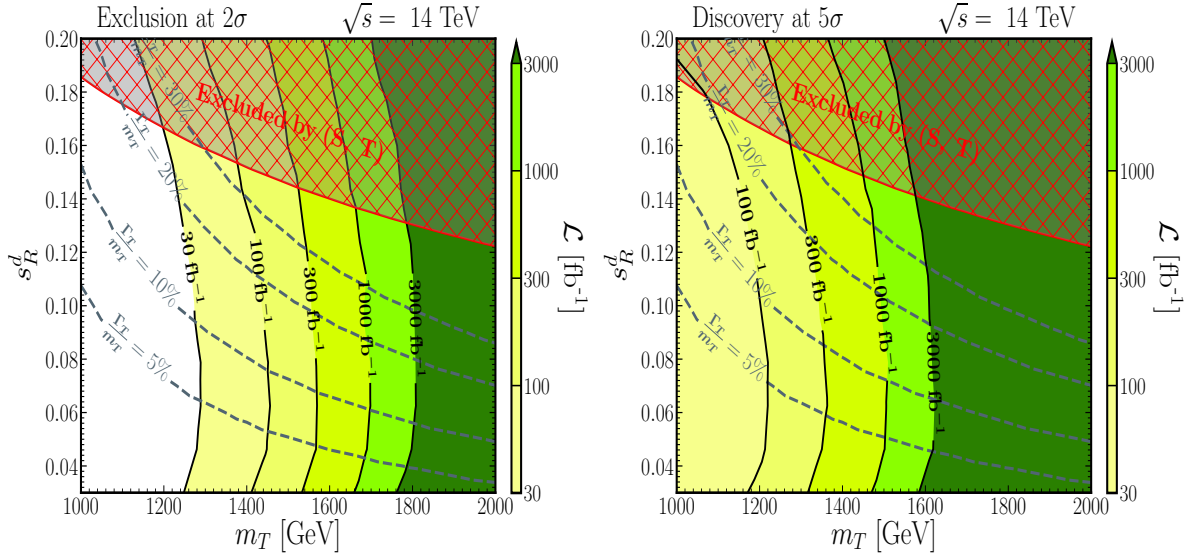


FIGURE 6: The exclusion limits (at 2σ) (left) and discovery prospects (at 5σ) (right) contour plots for the signal in $(m_T, \sin \theta_R^d)$ plane at $\sqrt{s} = 14$ TeV LHC for different integrated luminosities. Parameters used: $s_R^u = 0.05$, $\tan \beta = 2.6$, $m_H \sim m_A \sim m_{H^\pm} = 600$ GeV, and $m_{12}^2 = m_A^2 \tan \beta / (1 + \tan \beta^2)$.

In Fig. 6, we present the 2σ exclusion limits (left panel) and the 5σ discovery potential (right) in the $(m_T, \sin \theta_R^d)$ plane at a center-of-mass energy of $\sqrt{s} = 14$ TeV. The solid lines represent different integrated luminosities, while the dashed lines illustrate the width-to-mass ratios

Γ_T/m_T . When considering the narrow width approximation (NWA), where $\Gamma_T/m_T \leq 10\%$, the regions of exclusion and discovery are notably reduced. For an integrated luminosity of 100 fb^{-1} , the excluded region is $s_R^d \in [0, 0.08]$ with $m_T \in [1400, 1450] \text{ GeV}$, and the discovered region is $s_R^d \in [0, 0.11]$ with $m_T \in [1160, 1220] \text{ GeV}$. Increasing the luminosity to 300 fb^{-1} , the excluded region adjusts to $s_R^d \in [0, 0.07]$ with $m_T \in [1530, 1570] \text{ GeV}$, and the discovered region to $s_R^d \in [0, 0.09]$ with $m_T \in [1320, 1360] \text{ GeV}$. At 1000 fb^{-1} luminosity, the exclusion range tightens to $s_R^d \in [0, 0.06]$ with $m_T \in [1660, 1700] \text{ GeV}$, while the discovery region expands to $s_R^d \in [0, 0.074]$ with $m_T \in [1460, 1510] \text{ GeV}$. Finally, with an integrated luminosity of 3000 fb^{-1} , the exclusion region further narrows to $s_R^d \in [0, 0.056]$ with $m_T \in [1760, 1810] \text{ GeV}$, and the discovery region becomes $s_R^d \in [0, 0.066]$ with $m_T \in [1580, 1630] \text{ GeV}$.

• 5b Analysis

In the $5b$ analysis, we concentrate on primary irreducible backgrounds that arise from events with five high transverse momentum (p_T) b -tagged jets. The dominant backgrounds include $2b3j$, $4bj$, $2t2bj$, and $6b$, where some jets are misidentified as b -jets. Other potential backgrounds, such as $4t2b$, $4b2t$, and $2t3j$, have negligible cross-sections and are therefore excluded from the analysis.

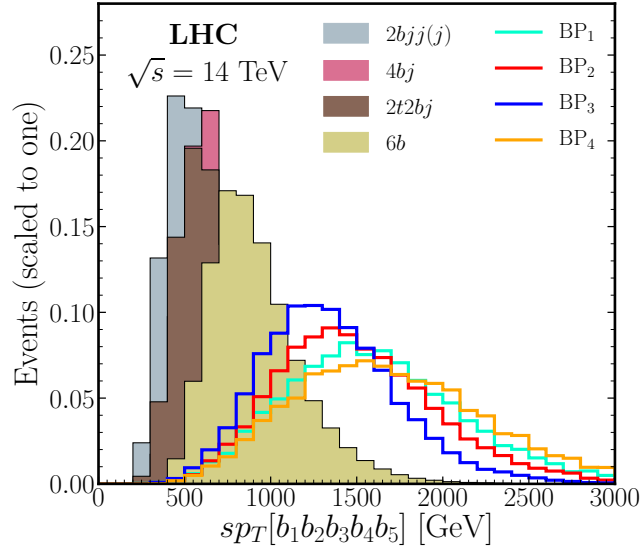


FIGURE 7: sp_T distribution for the signal BPs and backgrounds in the $5b$ analysis.

Fig. 7 shows the sp_T distribution for both the signal and the backgrounds in the $5b$ analysis. To enhance the signal significance, we apply a series of cuts as detailed in Table 7.

Cuts	Definition
Cut 1	$\Delta R(b, b) > 0.4$, $\eta(b) < 2.5$
Cut 2	$sp_T > 1500 \text{ GeV}$
Cut 3	$p_T^{b_4} > 120 \text{ GeV}$

TABLE 7: Set of cuts for the analysis of signal and background events at $\sqrt{s} = 14 \text{ TeV}$.

Table 8 summarizes the application of cut flows to both signal BPs and background events

at a center-of-mass energy of $\sqrt{s} = 14$ TeV. The results highlight the capability of the chosen cuts in reducing background interference and isolating the signal. After applying these cuts systematically, the total cut efficiency for the signal achieves values of 7.70%, 10%, 10.7%, and 10.9% for the distinct BPs (BP₁, BP₂, BP₃, and BP₄), respectively. Conversely, the cumulative efficiencies for background events are significantly reduced, approaching 1%.

Cuts	Signals				Backgrounds			
	BP1	BP2	BP3	BP4	$2bjets$	$4bj$	$2t2bj$	$6b$
Basic	9.92	1.92	0.74	0.27	309679.46	613.60	288.02	0.38
Cut1	2.79	0.48	0.17	0.06	345.7	36.46	14.21	0.05
Cut 2	0.88	0.225	0.09	0.03	2	0.37	0.21	0.0018
Cut 3	0.76	0.19	0.079	0.03	1.15	0.29	0.14	0.0018
Efficiency	7.70%	10%	10.7%	10.9%	$3.71E^{-6}$	$3.90E^{-4}$	$4.90E^{-4}$	1.24%

TABLE 8: Cut flow of the cross sections (in fb) for the signals and SM backgrounds at the LHC with $\sqrt{s}=14$ TeV with our three typical BPs .

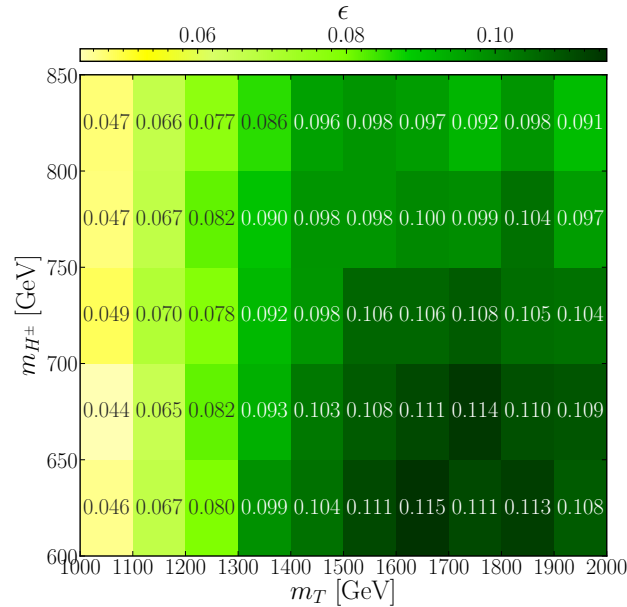


FIGURE 8: Similar to Fig. 5 but for 5b analysis.

In the context of the 5b analysis, Fig. 8 provides a concise representation of the selection efficiencies relevant to our signal, similar to the previous section. The visualization is depicted in the (m_T, m_{H^\pm}) plane with fixed parameters: $m_H = m_A = 600$ GeV, $\tan \beta = 6$, $s_R^u = 0.05$, and $s_R^d = 0.1$. The figure demonstrates an increase in efficiency as m_T increases while maintaining a relatively constant m_{H^\pm} . Peak efficiency values are concentrated within the m_{H^\pm} mass range of [600, 700] GeV, with the highest efficiencies observed for m_T between [1600, 1900] GeV.

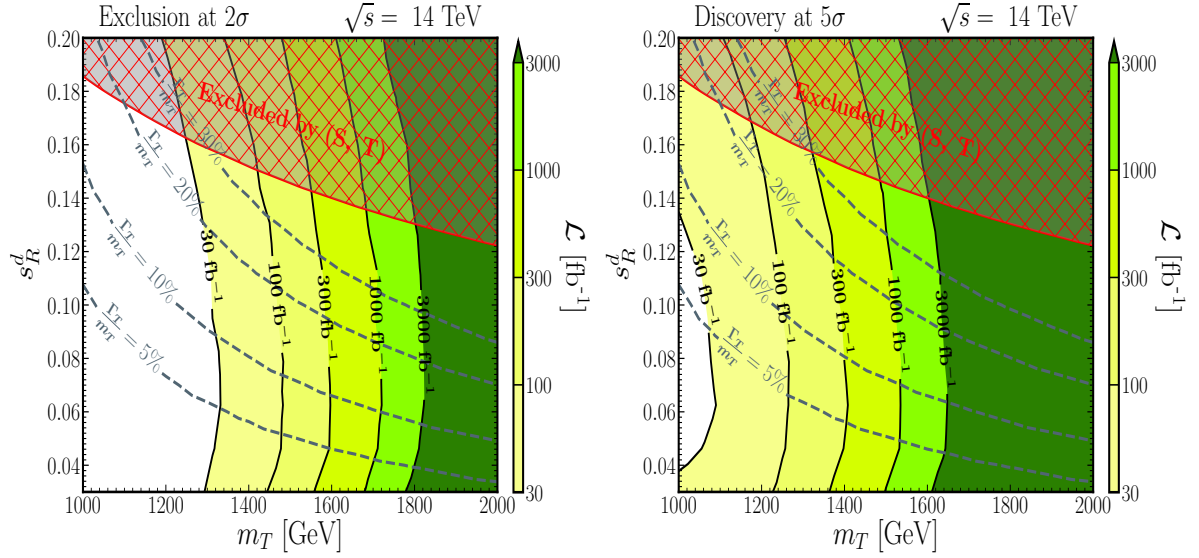


FIGURE 9: Similar to Fig. 6 but for 5b analysis.

Similar to the previous section, Fig. 9 illustrates the 2σ exclusion limits (left) and the 5σ discovery capability (right) in the (m_T, s_R^d) plane at a center-of-mass energy of $\sqrt{s} = 14$ TeV, assuming the ideal case of no systematic uncertainties ($\delta = 0$)⁶. The plot presents different integrated luminosities through solid lines, and dashed lines depict the contours based on the ratio Γ_T/m_T . Upon analyzing the figure and following similar steps as in the previous section, we discuss the regions that satisfy the condition $\Gamma_T/m_T \leq 10\%$. For an integrated luminosity of 100 fb^{-1} , the excluded region is $s_R^d \in [0, 0.076]$ with $m_T \in [1440, 1480]$ GeV, and the discovered region is $s_R^d \in [0, 0.1]$ with $m_T \in [1220, 1260]$ GeV. Increasing the luminosity to 300 fb^{-1} , the excluded region adjusts to $s_R^d \in [0, 0.068]$ with $m_T \in [1560, 1600]$ GeV, and the discovered region to $s_R^d \in [0, 0.084]$ with $m_T \in [1360, 1410]$ GeV. At 1000 fb^{-1} luminosity, the exclusion range tightens to $s_R^d \in [0, 0.06]$ with $m_T \in [1680, 1720]$ GeV, while the discovery region expands to $s_R^d \in [0, 0.074]$ with $m_T \in [1500, 1540]$ GeV. Finally, with an integrated luminosity of 3000 fb^{-1} , the exclusion region further narrows to $s_R^d \in [0, 0.056]$ with $m_T \in [1780, 1830]$ GeV, and the discovery region becomes $s_R^d \in [0, 0.066]$ with $m_T \in [1610, 1650]$ GeV.

5 Conclusion

In this study, we explored the potential of the 2HDM-II extended with VLQs to produce distinct signatures at the LHC. We focused on the production and decay channels involving the charged Higgs boson (H^\pm) and vector-like top (T) quarks, specifically through the process $pp \rightarrow T\bar{T} \rightarrow bH^+\bar{b}H^- \rightarrow b(tb)\bar{b}(\bar{t}\bar{b})$, resulting in final states rich in b -quarks. We conducted detailed signal-background analyses for two scenarios: tagging four b -jets (4b analysis) and tagging five b -jets (5b analysis). The analyses incorporated limits from EWPOs and constraints on the width-to-mass ratio ($\Gamma_T/m_T < 10\%$). We presented the discovery prospects and exclusion limits for the VLT using a range of integrated luminosities from 30 fb^{-1} to 3000 fb^{-1} .

Our findings underscore the extended 2HDM-II with VLQs as a powerful framework to uncover

⁶The results with a 10% systematic uncertainty is presented in Appendix 5.

new physics at the LHC, providing a promising pathway for the exclusion and discovery of VLT and charged Higgs bosons.

Appendix

Impact of $\delta = 10\%$ Systematic Uncertainty

This appendix evaluates the impact of a 10% systematic uncertainty on the exclusion and discovery limits for our analysis, focusing on the $5b$ analysis. Fig. 10 compares the 2σ exclusion limits and 5σ discovery prospects with a 10% systematic uncertainty (dashed red lines) for integrated luminosities of $\mathcal{L} = 300 \text{ fb}^{-1}$ and 3000 fb^{-1} against the ideal case without systematic uncertainty (solid black lines).

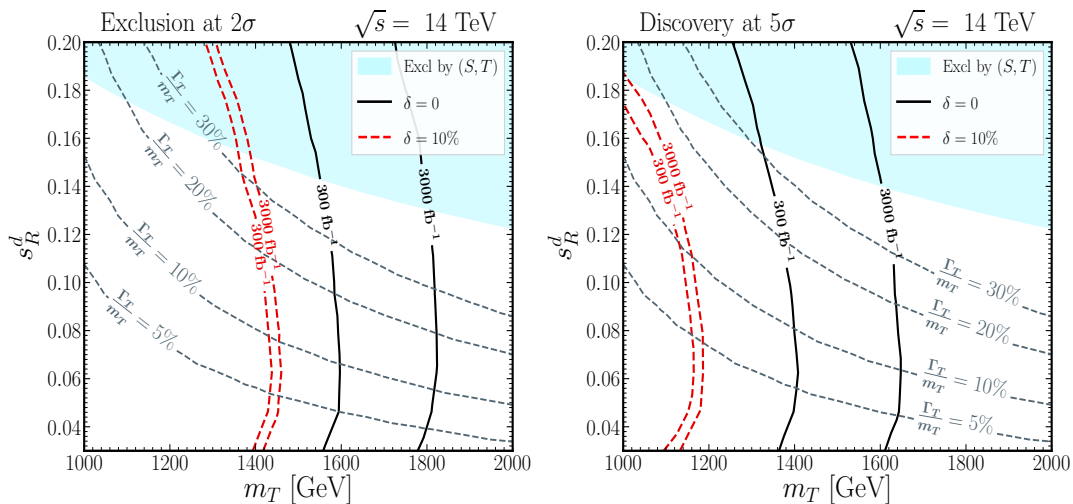


FIGURE 10: The discovery prospects (at 5σ) (left) and the exclusion limits (at 2σ) (right) contour plots for the signal in $(m_T, \sin\theta_R^d)$ plane at the LHC with $\sqrt{s} = 14 \text{ TeV}$ for two integrated luminosities: 300 fb^{-1} and 3000 fb^{-1} . Parameters used: $s_R^u = 0.05$, $\tan\beta = 2.6$, $m_H \sim m_A \sim m_{H^\pm} = 600 \text{ GeV}$, and $m_{12}^2 = m_A^2 \tan\beta / (1 + \tan\beta^2)$. The solid black lines indicate the ideal case without systematic uncertainty, while the dashed red lines indicate the results with $\delta = 10\%$. The light blue area represents the excluded region by (S, T) .

From both panels, it is evident that with a 10% systematic uncertainty and assuming the NWA, the excluded region for T at an integrated luminosity of $\mathcal{L} = 300 \text{ fb}^{-1}$ adjusts to $s_R^d \in [0, 0.08]$ with $m_T \in [1400, 1430] \text{ GeV}$, and the discovered region to $s_R^d \in [0, 0.084]$ with $m_T \in [1100, 1150] \text{ GeV}$. At a luminosity of 3000 fb^{-1} , the exclusion range tightens to $s_R^d \in [0, 0.076]$ with $m_T \in [1420, 1460] \text{ GeV}$, while the discovery region expands to $s_R^d \in [0, 0.115]$ with $m_T \in [1130, 1185] \text{ GeV}$.

References

- [1] A. Davidson and K.C. Wali, *Family Mass Hierarchy From Universal Seesaw Mechanism*, *Phys. Rev. Lett.* **60** (1988) 1813.
- [2] K.S. Babu and R.N. Mohapatra, *A Solution to the Strong CP Problem Without an Axion*, *Phys. Rev. D* **41** (1990) 1286.

- [3] B. Grinstein, M. Redi and G. Villadoro, *Low Scale Flavor Gauge Symmetries*, *JHEP* **11** (2010) 067 [[1009.2049](#)].
- [4] D. Guadagnoli, R.N. Mohapatra and I. Sung, *Gauged Flavor Group with Left-Right Symmetry*, *JHEP* **04** (2011) 093 [[1103.4170](#)].
- [5] T. Moroi and Y. Okada, *Radiative corrections to Higgs masses in the supersymmetric model with an extra family and antifamily*, *Mod. Phys. Lett. A* **7** (1992) 187.
- [6] T. Moroi and Y. Okada, *Upper bound of the lightest neutral Higgs mass in extended supersymmetric Standard Models*, *Phys. Lett. B* **295** (1992) 73.
- [7] K.S. Babu, I. Gogoladze, M.U. Rehman and Q. Shafi, *Higgs Boson Mass, Sparticle Spectrum and Little Hierarchy Problem in Extended MSSM*, *Phys. Rev. D* **78** (2008) 055017 [[0807.3055](#)].
- [8] S.P. Martin, *Extra vector-like matter and the lightest Higgs scalar boson mass in low-energy supersymmetry*, *Phys. Rev. D* **81** (2010) 035004 [[0910.2732](#)].
- [9] P.W. Graham, A. Ismail, S. Rajendran and P. Saraswat, *A Little Solution to the Little Hierarchy Problem: A Vector-like Generation*, *Phys. Rev. D* **81** (2010) 055016 [[0910.3020](#)].
- [10] S.P. Martin, *Raising the Higgs Mass with Yukawa Couplings for Isotriplets in Vector-Like Extensions of Minimal Supersymmetry*, *Phys. Rev. D* **82** (2010) 055019 [[1006.4186](#)].
- [11] J.L. Rosner, *E_6 and Exotic Fermions*, *Comments Nucl. Part. Phys.* **15** (1986) 195.
- [12] R.W. Robinett, *On the Mixing and Production of Exotic Fermions in E_6* , *Phys. Rev. D* **33** (1986) 1908.
- [13] N. Arkani-Hamed, A.G. Cohen, E. Katz and A.E. Nelson, *The Littlest Higgs*, *JHEP* **07** (2002) 034 [[hep-ph/0206021](#)].
- [14] M. Schmaltz and D. Tucker-Smith, *Little Higgs review*, *Ann. Rev. Nucl. Part. Sci.* **55** (2005) 229 [[hep-ph/0502182](#)].
- [15] B.A. Dobrescu and C.T. Hill, *Electroweak symmetry breaking via top condensation seesaw*, *Phys. Rev. Lett.* **81** (1998) 2634 [[hep-ph/9712319](#)].
- [16] R.S. Chivukula, B.A. Dobrescu, H. Georgi and C.T. Hill, *Top Quark Seesaw Theory of Electroweak Symmetry Breaking*, *Phys. Rev. D* **59** (1999) 075003 [[hep-ph/9809470](#)].
- [17] H.-J. He, C.T. Hill and T.M.P. Tait, *Top Quark Seesaw, Vacuum Structure and Electroweak Precision Constraints*, *Phys. Rev. D* **65** (2002) 055006 [[hep-ph/0108041](#)].
- [18] C.T. Hill and E.H. Simmons, *Strong Dynamics and Electroweak Symmetry Breaking*, *Phys. Rept.* **381** (2003) 235 [[hep-ph/0203079](#)].
- [19] K. Agashe, R. Contino and A. Pomarol, *The Minimal composite Higgs model*, *Nucl. Phys. B* **719** (2005) 165 [[hep-ph/0412089](#)].
- [20] R. Contino, L. Da Rold and A. Pomarol, *Light custodians in natural composite Higgs models*, *Phys. Rev. D* **75** (2007) 055014 [[hep-ph/0612048](#)].
- [21] R. Barbieri, B. Bellazzini, V.S. Rychkov and A. Varagnolo, *The Higgs boson from an extended symmetry*, *Phys. Rev. D* **76** (2007) 115008 [[0706.0432](#)].
- [22] C. Anastasiou, E. Furlan and J. Santiago, *Realistic Composite Higgs Models*, *Phys. Rev. D* **79** (2009) 075003 [[0901.2117](#)].
- [23] R. Benbrik et al., *Signatures of vector-like top partners decaying into new neutral scalar or pseudoscalar bosons*, *JHEP* **05** (2020) 028 [[1907.05929](#)].
- [24] J.A. Aguilar-Saavedra, *Identifying top partners at LHC*, *JHEP* **11** (2009) 030 [[0907.3155](#)].
- [25] Y. Okada and L. Panizzi, *LHC signatures of vector-like quarks*, *Adv. High Energy Phys.* **2013** (2013) 364936 [[1207.5607](#)].
- [26] A. De Simone, O. Matsedonskyi, R. Rattazzi and A. Wulzer, *A First Top Partner Hunter's Guide*, *JHEP* **04** (2013) 004 [[1211.5663](#)].

- [27] M. Buchkremer, G. Cacciapaglia, A. Deandrea and L. Panizzi, *Model Independent Framework for Searches of Top Partners*, *Nucl. Phys. B* **876** (2013) 376 [[1305.4172](#)].
- [28] J.A. Aguilar-Saavedra, R. Benbrik, S. Heinemeyer and M. Pérez-Victoria, *Handbook of vectorlike quarks: Mixing and single production*, *Phys. Rev. D* **88** (2013) 094010 [[1306.0572](#)].
- [29] B. Yang, Z. Li, X. Jia, S. Moretti and L. Shang, *Search for single vector-like B quark production in hadronic final states at the LHC*, [2405.13452](#).
- [30] L. Shang, Y. Yan, S. Moretti and B. Yang, *Single production of an exotic vectorlike Y quark at future high energy pp colliders*, *Phys. Rev. D* **109** (2024) 115016 [[2401.00770](#)].
- [31] L. Han, S. Wang, L. Shang and B. Yang, *Search for the singlet vector-like top quark in the channel with at hadron colliders**, *Chin. Phys. C* **47** (2023) 043108 [[2302.14642](#)].
- [32] B. Yang, X. Sima, S. Wang and L. Shang, *Single vectorlike top quark production in the tZ channel at high energy pp colliders*, *Phys. Rev. D* **105** (2022) 096010.
- [33] A. Deandrea, T. Flacke, B. Fuks, L. Panizzi and H.-S. Shao, *Single production of vector-like quarks: the effects of large width, interference and NLO corrections*, *JHEP* **08** (2021) 107 [[2105.08745](#)].
- [34] G. Cacciapaglia, A. Carvalho, A. Deandrea, T. Flacke, B. Fuks, D. Majumder et al., *Next-to-leading-order predictions for single vector-like quark production at the LHC*, *Phys. Lett. B* **793** (2019) 206 [[1811.05055](#)].
- [35] A. Carvalho, S. Moretti, D. O'Brien, L. Panizzi and H. Prager, *Single production of vectorlike quarks with large width at the Large Hadron Collider*, *Phys. Rev. D* **98** (2018) 015029 [[1805.06402](#)].
- [36] G. Cacciapaglia, A. Deandrea, N. Gaur, D. Harada, Y. Okada and L. Panizzi, *The LHC potential of Vector-like quark doublets*, *JHEP* **11** (2018) 055 [[1806.01024](#)].
- [37] A. Banerjee, V. Ellajosyula and L. Panizzi, *Heavy vector-like quarks decaying to exotic scalars: a case study with triplets*, *JHEP* **01** (2024) 187 [[2311.17877](#)].
- [38] A. Banerjee, E. Bergeaas Kuutmann, V. Ellajosyula, R. Enberg, G. Ferretti and L. Panizzi, *Vector-like quarks: status and new directions at the LHC*, [2406.09193](#).
- [39] Y.-B. Liu, B. Hu and C.-Z. Li, *Single production of vectorlike quarks with charge $5/3$ at the 14 TeV LHC*, [2402.01248](#).
- [40] J.-Z. Han, Y.-B. Liu and S.-Y. Xu, *Pair production of the singlet vector-like B quark at the CLIC*, *Eur. Phys. J. C* **84** (2024) 61 [[2401.11423](#)].
- [41] G.-S. Lv, X.-M. Cui, Y.-Q. Li and Y.-B. Liu, *Pair production of the vectorlike top partner at future muon collider*, *Nucl. Phys. B* **985** (2022) 116016.
- [42] X.-M. Cui, Y.-Q. Li and Y.-B. Liu, *Search for pair production of the heavy vectorlike top partner in same-sign dilepton signature at the HL-LHC*, *Phys. Rev. D* **106** (2022) 115025 [[2212.01514](#)].
- [43] L. Han, L.-F. Du and Y.-B. Liu, *Single production of vectorlike T quark at future high-energy linear $e+e-$ collider*, *Phys. Rev. D* **105** (2022) 115032 [[2206.06562](#)].
- [44] X.-Y. Tian, L.-F. Du and Y.-B. Liu, *Search for single production of vectorlike top partners through th channel at the HE-LHC and FCC-hh*, *Eur. Phys. J. C* **81** (2021) 594.
- [45] Y.-B. Liu and S. Moretti, *Search for single production of a top quark partner via the $T \rightarrow th$ and $h \rightarrow WW^*$ channels at the LHC*, *Phys. Rev. D* **100** (2019) 015025 [[1902.03022](#)].
- [46] Y.-B. Liu, *Search for single production of the heavy vectorlike T quark with $T \rightarrow th$ and $h \rightarrow \gamma\gamma$ at the high-luminosity LHC*, *Phys. Rev. D* **95** (2017) 035013 [[1612.05851](#)].
- [47] J.a.M. Alves, G.C. Branco, A.L. Cherchiglia, C.C. Nishi, J.T. Penedo, P.M.F. Pereira et al., *Vector-like singlet quarks: A roadmap*, *Phys. Rept.* **1057** (2024) 1 [[2304.10561](#)].

- [48] R. Dermíšek, E. Lunghi and S. Shin, *Hunting for Vectorlike Quarks*, *JHEP* **04** (2019) 019 [[1901.03709](#)].
- [49] R. Dermíšek, E. Lunghi, N. McGinnis and S. Shin, *Signals with six bottom quarks for charged and neutral Higgs bosons*, *JHEP* **07** (2020) 241 [[2005.07222](#)].
- [50] R. Dermíšek, E. Lunghi, N. McGinnis and S. Shin, *Tau-jet signatures of vectorlike quark decays to heavy charged and neutral Higgs bosons*, *JHEP* **08** (2021) 159 [[2105.10790](#)].
- [51] N. Vignaroli, *Discovering the composite Higgs through the decay of a heavy fermion*, *JHEP* **07** (2012) 158 [[1204.0468](#)].
- [52] N. Vignaroli, *Z-peaked excess from heavy gluon decays to vectorlike quarks*, *Phys. Rev. D* **91** (2015) 115009 [[1504.01768](#)].
- [53] N. Vignaroli, *$\Delta F=1$ constraints on composite Higgs models with LR parity*, *Phys. Rev. D* **86** (2012) 115011 [[1204.0478](#)].
- [54] R. Benbrik, M. Berrouj, M. Boukidi, A. Habjia, E. Ghourmin and L. Rahili, *Search for single production of vector-like top partner $T \rightarrow H^+b$ and $H^\pm \rightarrow tb$ at the LHC Run-III*, *Phys. Lett. B* **843** (2023) 138024.
- [55] J. Bardhan, T. Mandal, S. Mitra and C. Neeraj, *Machine learning-enhanced search for a vectorlike singlet B quark decaying to a singlet scalar or pseudoscalar*, *Phys. Rev. D* **107** (2023) 115001 [[2212.02442](#)].
- [56] A. Bhardwaj, K. Bhide, T. Mandal, S. Mitra and C. Neeraj, *Discovery prospects of a vectorlike top partner decaying to a singlet boson*, *Phys. Rev. D* **106** (2022) 075024 [[2204.09005](#)].
- [57] A. Bhardwaj, T. Mandal, S. Mitra and C. Neeraj, *Roadmap to explore vectorlike quarks decaying to a new scalar or pseudoscalar*, *Phys. Rev. D* **106** (2022) 095014 [[2203.13753](#)].
- [58] R. Benbrik and M. Boukidi, *Phenomenology of Heavy Quark at the LHC*, (2023), [DOI](#).
- [59] **ATLAS** collaboration, *Search for pair production of vector-like top quarks in events with one lepton, jets, and missing transverse momentum in $\sqrt{s} = 13$ TeV pp collisions with the ATLAS detector*, *JHEP* **08** (2017) 052 [[1705.10751](#)].
- [60] **ATLAS** collaboration, *Search for pair production of heavy vector-like quarks decaying to high- p_T W bosons and b quarks in the lepton-plus-jets final state in pp collisions at $\sqrt{s} = 13$ TeV with the ATLAS detector*, *JHEP* **10** (2017) 141 [[1707.03347](#)].
- [61] **ATLAS** collaboration, *Search for pair production of up-type vector-like quarks and for four-top-quark events in final states with multiple b-jets with the ATLAS detector*, *JHEP* **07** (2018) 089 [[1803.09678](#)].
- [62] **CMS** collaboration, *Search for pair production of vector-like T and B quarks in single-lepton final states using boosted jet substructure in proton-proton collisions at $\sqrt{s} = 13$ TeV*, *JHEP* **11** (2017) 085 [[1706.03408](#)].
- [63] **CMS** collaboration, *Search for pair production of vector-like quarks in the $bW\bar{b}W$ channel from proton-proton collisions at $\sqrt{s} = 13$ TeV*, *Phys. Lett. B* **779** (2018) 82 [[1710.01539](#)].
- [64] **CMS** collaboration, *Search for vector-like T and B quark pairs in final states with leptons at $\sqrt{s} = 13$ TeV*, *JHEP* **08** (2018) 177 [[1805.04758](#)].
- [65] **CMS** collaboration, *Search for single production of a vector-like T quark decaying to a Z boson and a top quark in proton-proton collisions at $\sqrt{s} = 13$ TeV*, *Phys. Lett. B* **781** (2018) 574 [[1708.01062](#)].
- [66] **CMS** collaboration, *Search for single production of vector-like quarks decaying to a b quark and a Higgs boson*, *JHEP* **06** (2018) 031 [[1802.01486](#)].
- [67] **ATLAS** collaboration, *Search for single production of vector-like quarks decaying into Wb in pp collisions at $\sqrt{s} = 13$ TeV with the ATLAS detector*, .

- [68] **ATLAS** collaboration, *Search for pair production of heavy vector-like quarks decaying into high- p_T W bosons and top quarks in the lepton-plus-jets final state in pp collisions at $\sqrt{s} = 13$ TeV with the ATLAS detector*, *JHEP* **08** (2018) 048 [[1806.01762](#)].
- [69] **ATLAS** collaboration, *Search for pair production of heavy vector-like quarks decaying into hadronic final states in pp collisions at $\sqrt{s} = 13$ TeV with the ATLAS detector*, *Phys. Rev. D* **98** (2018) 092005 [[1808.01771](#)].
- [70] **ATLAS** collaboration, *Combination of the searches for pair-produced vector-like partners of the third-generation quarks at $\sqrt{s} = 13$ TeV with the ATLAS detector*, *Phys. Rev. Lett.* **121** (2018) 211801 [[1808.02343](#)].
- [71] **ATLAS** collaboration, *Search for single production of vector-like quarks decaying into Wb in pp collisions at $\sqrt{s} = 13$ TeV with the ATLAS detector*, *JHEP* **05** (2019) 164 [[1812.07343](#)].
- [72] **ATLAS** collaboration, *Search for single production of vector-like T quarks decaying to Ht or Zt in pp collisions at $\sqrt{s} = 13$ TeV with the ATLAS detector*, .
- [73] **ATLAS** collaboration, *Search for single vector-like B quark production and decay via $B \rightarrow bH(b\bar{b})$ in pp collisions at $\sqrt{s} = 13$ TeV with the ATLAS detector*, .
- [74] **ATLAS** collaboration, *Search for pair-production of vector-like quarks in pp collision events at $\sqrt{s} = 13$ TeV with at least one leptonically-decaying Z boson and a third-generation quark with the ATLAS detector*, .
- [75] **CMS** collaboration, *Search for single production of a heavy vector-like T quark decaying to a Higgs boson and a top quark with a lepton and jets in the final state*, *Phys. Lett. B* **771** (2017) 80 [[1612.00999](#)].
- [76] **CMS** collaboration, *Search for single production of vector-like quarks decaying into a b quark and a W boson in proton-proton collisions at $\sqrt{s} = 13$ TeV*, *Phys. Lett. B* **772** (2017) 634 [[1701.08328](#)].
- [77] **CMS** collaboration, *Search for a vector-like quark decaying to a top quark and a W boson*, .
- [78] **CMS** collaboration, *Search for single production of vector-like quarks decaying to a top quark and a W boson in proton-proton collisions at $\sqrt{s} = 13$ TeV*, *Eur. Phys. J. C* **79** (2019) 90 [[1809.08597](#)].
- [79] **CMS** collaboration, *Search for a W' boson decaying to a vector-like quark and a top or bottom quark in the all-jets final state*, *JHEP* **03** (2019) 127 [[1811.07010](#)].
- [80] **CMS** collaboration, *A search for bottom-type, vector-like quark pair production in a fully hadronic mode in proton-proton collisions at $\sqrt{s} = 13$ TeV*, .
- [81] **CMS** collaboration, *A search for bottom-type, vector-like quark pair production in a fully hadronic final state in proton-proton collisions at $\sqrt{s} = 13$ TeV*, *Phys. Rev. D* **102** (2020) 112004 [[2008.09835](#)].
- [82] **CMS** collaboration, *Search for single production of a vector-like T quark decaying to a top quark and a Z boson in the final state with jets and missing transverse momentum at $\sqrt{s} = 13$ TeV*, *JHEP* **05** (2022) 093 [[2201.02227](#)].
- [83] **CMS** collaboration, *Search for a W' boson decaying to a vector-like quark and a top or bottom quark in the all-jets final state at $\sqrt{s} = 13$ TeV*, *JHEP* **09** (2022) 088 [[2202.12988](#)].
- [84] **CMS** collaboration, *Search for pair production of vector-like quarks in leptonic final states in proton-proton collisions at $\sqrt{s} = 13$ TeV*, [2209.07327](#).
- [85] G.C. Branco and M.N. Rebelo, *Vector-like Quarks*, *PoS DISCRETE2020-2021* (2022) 004 [[2208.07235](#)].
- [86] H. Abouabid, A. Arhrib, R. Benbrik, M. Boukidi and J.E. Falaki, *The oblique parameters in the 2HDM with vector-like quarks: confronting M_W CDF-II anomaly*, *J. Phys. G* **51** (2024) 075001 [[2302.07149](#)].

- [87] S.-P. He, *Leptoquark and vector-like quark extended model for simultaneous explanation of W boson mass and muon $g-2$ anomalies**, *Chin. Phys. C* **47** (2023) 043102 [2205.02088].
- [88] J. Cao, L. Meng, L. Shang, S. Wang and B. Yang, *Interpreting the W -mass anomaly in vectorlike quark models*, *Phys. Rev. D* **106** (2022) 055042 [2204.09477].
- [89] A. Arhrib, R. Benbrik, M. Boukidi and S. Moretti, *Anatomy of Vector-Like Bottom-Quark Models in the Alignment Limit of the 2-Higgs Doublet Model Type-II*, **2403.13021**.
- [90] A. Arhrib, R. Benbrik, M. Boukidi, B. Manaut and S. Moretti, *Anatomy of Vector-Like Top-Quark Models in the Alignment Limit of the 2-Higgs Doublet Model Type-II*, **2401.16219**.
- [91] R. Benbrik, M. Boukidi and S. Moretti, *Probing charged Higgs bosons in the two-Higgs-doublet model type II with vectorlike quarks*, *Phys. Rev. D* **109** (2024) 055016 [2211.07259].
- [92] G.C. Branco, P.M. Ferreira, L. Lavoura, M.N. Rebelo, M. Sher and J.P. Silva, *Theory and phenomenology of two-Higgs-doublet models*, *Phys. Rept.* **516** (2012) 1 [1106.0034].
- [93] J.F. Gunion, H.E. Haber, G.L. Kane and S. Dawson, *The Higgs Hunter's Guide*, vol. 80 (2000).
- [94] M.E. Peskin and T. Takeuchi, *Estimation of oblique electroweak corrections*, *Phys. Rev. D* **46** (1992) 381.
- [95] G. Altarelli and R. Barbieri, *Vacuum polarization effects of new physics on electroweak processes*, *Phys. Lett. B* **253** (1991) 161.
- [96] F. Boudjema, A. Djouadi and C. Verzegnassi, *A General Sum Rule for the Top Mass From b Physics on Z Resonance*, *Phys. Lett. B* **238** (1990) 423.
- [97] S. Kanemura, T. Kubota and E. Takasugi, *Lee-Quigg-Thacker bounds for Higgs boson masses in a two doublet model*, *Phys. Lett. B* **313** (1993) 155 [hep-ph/9303263].
- [98] A. Barroso, P.M. Ferreira, I.P. Ivanov and R. Santos, *Metastability bounds on the two Higgs doublet model*, *JHEP* **06** (2013) 045 [1303.5098].
- [99] N.G. Deshpande and E. Ma, *Pattern of Symmetry Breaking with Two Higgs Doublets*, *Phys. Rev. D* **18** (1978) 2574.
- [100] W. Grimus, L. Lavoura, O.M. Ogreid and P. Osland, *A Precision constraint on multi-Higgs-doublet models*, *J. Phys. G* **35** (2008) 075001 [0711.4022].
- [101] M.J. Molewski and B.J.P. Jones, *Scalable qubit representations of neutrino mixing matrices*, *Phys. Rev. D* **105** (2022) 056024 [2111.05401].
- [102] D. Eriksson, J. Rathsmann and O. Stal, *2HDMC: Two-Higgs-Doublet Model Calculator Physics and Manual*, *Comput. Phys. Commun.* **181** (2010) 189 [0902.0851].
- [103] P. Bechtle, D. Dercks, S. Heinemeyer, T. Klingl, T. Stefaniak, G. Weiglein et al., *HiggsBounds-5: Testing Higgs Sectors in the LHC 13 TeV Era*, *Eur. Phys. J. C* **80** (2020) 1211 [2006.06007].
- [104] P. Bechtle, S. Heinemeyer, T. Klingl, T. Stefaniak, G. Weiglein and J. Wittbrodt, *HiggsSignals-2: Probing new physics with precision Higgs measurements in the LHC 13 TeV era*, *Eur. Phys. J. C* **81** (2021) 145 [2012.09197].
- [105] H. Bahl, T. Biekötter, S. Heinemeyer, C. Li, S. Paasch, G. Weiglein et al., *HiggsTools: BSM scalar phenomenology with new versions of HiggsBounds and HiggsSignals*, *Comput. Phys. Commun.* **291** (2023) 108803 [2210.09332].
- [106] P. Bechtle, O. Brein, S. Heinemeyer, G. Weiglein and K.E. Williams, *HiggsBounds: Confronting Arbitrary Higgs Sectors with Exclusion Bounds from LEP and the Tevatron*, *Comput. Phys. Commun.* **181** (2010) 138 [0811.4169].

- [107] P. Bechtle, O. Brein, S. Heinemeyer, G. Weiglein and K.E. Williams, *HiggsBounds 2.0.0: Confronting Neutral and Charged Higgs Sector Predictions with Exclusion Bounds from LEP and the Tevatron*, *Comput. Phys. Commun.* **182** (2011) 2605 [[1102.1898](#)].
- [108] P. Bechtle, O. Brein, S. Heinemeyer, O. Stål, T. Stefaniak, G. Weiglein et al., *HiggsBounds – 4: Improved Tests of Extended Higgs Sectors against Exclusion Bounds from LEP, the Tevatron and the LHC*, *Eur. Phys. J. C* **74** (2014) 2693 [[1311.0055](#)].
- [109] P. Bechtle, S. Heinemeyer, O. Stal, T. Stefaniak and G. Weiglein, *Applying Exclusion Likelihoods from LHC Searches to Extended Higgs Sectors*, *Eur. Phys. J. C* **75** (2015) 421 [[1507.06706](#)].
- [110] J. Alwall, R. Frederix, S. Frixione, V. Hirschi, F. Maltoni, O. Mattelaer et al., *The automated computation of tree-level and next-to-leading order differential cross sections, and their matching to parton shower simulations*, *JHEP* **07** (2014) 079 [[1405.0301](#)].
- [111] J. Pumplin, D.R. Stump, J. Huston, H.L. Lai, P.M. Nadolsky and W.K. Tung, *New generation of parton distributions with uncertainties from global QCD analysis*, *JHEP* **07** (2002) 012 [[hep-ph/0201195](#)].
- [112] A. Alloul, N.D. Christensen, C. Degrande, C. Duhr and B. Fuks, *FeynRules 2.0 - A complete toolbox for tree-level phenomenology*, *Comput. Phys. Commun.* **185** (2014) 2250 [[1310.1921](#)].
- [113] C. Degrande, C. Duhr, B. Fuks, D. Grellscheid, O. Mattelaer and T. Reiter, *UFO - The Universal FeynRules Output*, *Comput. Phys. Commun.* **183** (2012) 1201 [[1108.2040](#)].
- [114] T. Sjöstrand, S. Ask, J.R. Christiansen, R. Corke, N. Desai, P. Ilten et al., *An introduction to PYTHIA 8.2*, *Comput. Phys. Commun.* **191** (2015) 159 [[1410.3012](#)].
- [115] **DELPHES 3** collaboration, *DELPHES 3, A modular framework for fast simulation of a generic collider experiment*, *JHEP* **02** (2014) 057 [[1307.6346](#)].
- [116] M. Cacciari, G.P. Salam and G. Soyez, *The anti- k_t jet clustering algorithm*, *JHEP* **04** (2008) 063 [[0802.1189](#)].
- [117] **CMS** collaboration, *Identification of b-Quark Jets with the CMS Experiment*, *JINST* **8** (2013) P04013 [[1211.4462](#)].
- [118] M. Czakon and A. Mitov, *Top++: A Program for the Calculation of the Top-Pair Cross-Section at Hadron Colliders*, *Comput. Phys. Commun.* **185** (2014) 2930 [[1112.5675](#)].
- [119] G. Bevilacqua, M. Czakon, M. Krämer, M. Kubocz and M. Worek, *Quantifying quark mass effects at the LHC: A study of $pp \rightarrow b\bar{b}b\bar{b} + X$ at next-to-leading order*, *JHEP* **07** (2013) 095 [[1304.6860](#)].
- [120] G. Bevilacqua, M. Czakon, C.G. Papadopoulos, R. Pittau and M. Worek, *Assault on the NLO Wishlist: $pp \rightarrow t$ anti- t b anti- b* , *JHEP* **09** (2009) 109 [[0907.4723](#)].
- [121] G. Bevilacqua and M. Worek, *Constraining BSM Physics at the LHC: Four top final states with NLO accuracy in perturbative QCD*, *JHEP* **07** (2012) 111 [[1206.3064](#)].
- [122] A. Papaefstathiou, G. Tetlalmatzi-Xolocotzi and M. Zaro, *Triple Higgs boson production to six b-jets at a 100 TeV proton collider*, *Eur. Phys. J. C* **79** (2019) 947 [[1909.09166](#)].
- [123] G. Cowan, K. Cranmer, E. Gross and O. Vitells, *Asymptotic formulae for likelihood-based tests of new physics*, *Eur. Phys. J. C* **71** (2011) 1554 [[1007.1727](#)].